Effect of Heat Sources on Non-Darcy Convective Heat and Mass Transfer Flow of CuO-Water and Al_2O_3-Water Nanofluids in Vertical Channel

C. Sulochana[#1] G.N. Ramakrishna[#2]
#1Professor, Department of Mathematics, Gulbarga University, Gulbarga, India
#2Research Scholar, Department of Mathematics, Gulbarga University, Gulbarga-India

ABSTRACT: We analyze the effect of heat sources on non-Darcy mixed convective heat and mass transfer flow of nanofluid in a vertical channel. The non-linear coupled equations governing the flow heat and mass transfer flow have been analyzed by Galerkin Finite element analysis with quadratic approximation functions. It is found that the Velocity, actual temperature and Concentration enhances with nanoparticle volume fraction ϕ. The Velocity and actual temperature reduces with increase in Forchheimer number $\Delta \leq 4$ and enhances with higher $\Delta \geq 6$.

Key Words: Nanofluid, non-Darcy, Heat sources, CuO-Water, Al_2O_3-Water, Vertical Channel,

Corresponding Author: G. N. RAMA KRISHNA

1. INTRODUCTION

Nanotechnology has been broadly utilized in several commercial applications. That aims at manipulating the structure of the make a difference at the molecular degree with the goal for innovation in practically every industry and public practice including biological sciences, physical sciences electronics cooling, vehicles, the environment and national security [5]. Low thermal conductivity of conventional heat transfer fluids such as water, oil and ethylene glycol mixture is a primary limitation in enhancing the performance and the compactness of many engineering electronic devices. To overcome this drawback, there is a strong motivation to develop advanced heat transfer fluids with substantially higher conductivities to enhance thermal characteristics. Small particles (nanoparticles) stay suspended much longer than larger particles. If particles settle rapidly (micro particles), more particles need to be added to replace the settled particles, resulting in extra cost and degradation in the heat transfer enhancement. As such an innovative way in improving thermal conductivities of a fluid is to suspend metallic nanoparticles within it. The resulting mixture referred to as a nanofluid possesses a substantially larger thermal conductivity compared to that of traditional fluids. Nanofluids demonstrate anomalously high thermal conductivity, significant change in properties such as viscosity and specific heat in comparison to the base fluid, features which have attracted many researchers to perform in engineering applications. The popularity of nanofluids can be gauged from the researches done by scientists for its frequent applications and can be found in the literature [3, 6, 7, 9, 13, 15, 16, 29-31, 33, 37, 40].

The Darcy law is used broadly for the problem of flow in porous media. It is valid only slow in porous media. It is an important to note that Darcy law is inadequate for high

flow velocities and porous material of large pore radii, the inertial effects become significant. Flor this flow situation, the relation between pressure drop and the velocity is non-linear. In general, we must consider the effect of the fluid inertia, as well as viscous diffusion which may well become significant for materials with very high porosities such as fibrous and foams. The Darcy-Forchheimer model was employed by many investigators [1, 4, 10, 14, 22, 25, 26, 35, 38-39 43].

The Brinkman – Extended – Darcy modal was considered in Tong and Subramanian [36] and Lauriat and Prasad [17] to examine the boundary effects on free convection in a vertical cavity. While Tong and Subramanian performed a Weber – type boundary layer analysis, Lauriat and Prasad solved the problem numerically for A=1 and5. It was shown that for a fixed modified Rayleigh number, Ra, the Nusselt number; decrease with an increase in the Darcy number; the reduction being larger at higher values of Ra. A numerical study based on the Forchheimer-Brinkman-Extended Darcy equation of motion has also been reported recently by Beckerman et al [2]. They demonstrated that the inclusion of both the inertia and boundary effects is important for convection in a rectangular packed – sphere cavity.

The vertical channel is an often encountered configuration in thermal engineering equipment, as an example, collectors of solar power, cooling devices of digital and micro-digital equipments and many others. The investigation of nanofluid in vertical channel has been made by several authors. Maïga et al. [20] have analyzed the heat transfer behaviors of nanofluids in a uniformly heated tube. Maïga et al. [21] have studied the heat transfer enhancement by using nano- fluids in forced convection flows. Polidori et al. [24] have presented the heat transfer modeling of Newtonian nanofluids in laminar free convection. Hang and Pop [49] have examined the fully developed mixed convection flow in a vertical channel filled with nanofluids. Maghrebi et al. [19] have studied the forced convective heat transfer of nanofluids in a porous channel. Grosan and Pop [12] have presented the fully developed mixed convection in a vertical channel filled with nanofluid. Sacheti et al. [28] have studied the transient free convective flow of a nanofluid in a vertical channel. Fakour et al [11] have described the mixed convection flow of a nanofluid in a vertical channel. Nield and Kuznetsov [23] have discussed the forced convection in a channel occupied by a nanofluid. The magnetohydrodynamic flow in a permeable channel filled with nanofluid has been investigated by Sheikholeslami and Ganji [32]. Rossi di Schio [27] has examined the effect of Brownian diffusion and thermophoresis on the laminar forced convection of a nanofluid in a channel. Xu et al. [42] have analyzed the mixed convection flow of a nanofluid in a vertical channel. Das et al [8] have studied the mixed convective magnetohydrodynamic flow in a vertical channel filled with nanofluid. Recently Madhusudhana Reddy et al [18] have analyzed Finite element analysis of mixed convective heat and mass transfer flow of nanofluid in vertical channel.

Keeping the above application in view we made an attempt to study non-Darcy convective heat and Mass transfer flow of a nanofluid in a vertical channel with heat generating sources. The Brinkman Forchheimer extended a Darcy equation which takes into account the boundary and inertia effects are used in the governing linear momentum equation. The effect of density variation is combined to the buoyancy term under Boussinesq approximation. The momentum, energy and diffusion equations are coupled equations. In order to obtain a better insight into this complex problem, we make use of Galerkin finite element analysis with Quadratic Polynomial approximations. The Galerkin finite element analysis has two important features. The first is that the approximation solution is written directly as a linear combination of approximation functions with unknown nodal values as coefficients. Secondly, the approximation polynomials are chosen exclusively from the lower order Piecewise polynomials restricted to contiguous elements. The velocity, temperature,

concentration, shear stress and rate of Heat and Mass transfer are evaluated numerically for different variations of parameter.

2. FORMULATION OF THE PROBLEM

We investigate a fully developed laminar convective heat and mass transfer flow of a nanofluid through a porous medium confined in a vertical channel bounded by flat walls. We choose a Cartesian co-ordinate system O(x, y, z) with x- axis in the vertical direction and y-axis normal to the walls. The walls are taken at y= ± L. The walls are maintained at constant temperature and concentration. A constant axial pressure gradient is also imposed so that this resultant flow is a mixed convection flow. The Brinkman-Forchheimer-extended Darcy equation which account for boundary inertia effects in the momentum equation is used to obtain the velocity field.

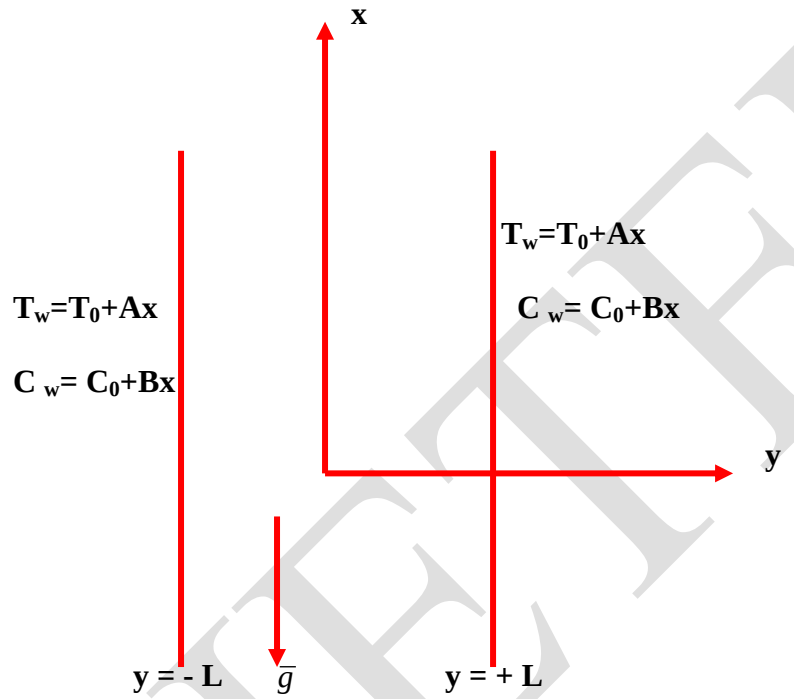

Fig1: Configuration of the problem

$$\nabla.\bar{q} = 0 \qquad (Equation\ of\ \ continuity) \tag{1}$$

$$\frac{\rho_{nf}}{\delta}\frac{\partial \bar{q}}{\partial t} + \frac{\rho_{nf}}{\delta^2}(\bar{q}.\nabla)\bar{q} = -\nabla p + \rho_{nf}\bar{g} - \frac{\rho_{nf}F}{\sqrt{k}}|\bar{q}|.\bar{q} + \mu_{nf}\nabla^2 q - \left(\frac{\mu}{k}\right)\bar{q} \tag{2}$$

$(Equation\ of\ \ linear\ momentum)$

$$(\rho C_p)_{nf}\left(\frac{\partial T}{\partial t} + (\bar{q}.\nabla)T\right) = k_{nf}\nabla^2 T + Q(T_o - T) \quad (Equation\ of\ \ energy) \tag{3}$$

$$\frac{\partial C}{\partial t} + (\bar{q}.\nabla)C = D_1\nabla^2 C - k_1 C + k_{11}\nabla^2 T \qquad (Equation\ of\ diffusion) \tag{4}$$

$$\rho - \rho_0 = -\beta\rho_0(T - T_0) - \beta^{\bullet}\rho_0(C - C_0) \qquad (Equation\ of\ \ State) \tag{5}$$

where u is the velocity component, T and C are the temperature and Concentration, p is the pressure ,ρ is the density of the fluid ,Cp is the specific heat at constant pressure, μ is the coefficient of viscosity, k is the permeability of the porous medium, δ is the porosity of the medium,β is the coefficient of thermal expansion ,k_f is the coefficient of thermal

conductivity, F is a function that depends on the Reynolds number and the microstructure of porous medium, $\beta^{\bullet}$ is the volumetric coefficient of expansion with mass fraction concentration, k_1 is the chemical reaction coefficient and D_1 is the chemical molecular diffusivity and Q is the strength of the heat generating source. Here, the thermo physical properties of the solid and fluid have been assumed to be constant except for the density variation in the body force term (Boussinesq approximation) and the solid particles and the fluid is considered to be in the thermal equilibrium).

The effective density of the nanofluid is given by

$$\rho_{nf} = (1-\varphi)\rho_f + \varphi\rho_s \quad (6)$$

Where ϕ is the solid volume fraction of nanoparticles

Thermal diffusivity of the nanofluid is

$$\alpha_{nf} = \frac{k_{nf}}{(\rho C_p)_{nf}} \quad (7)$$

Where the heat capacitance C_p of the nanofluid is obtained as

$$(\rho C_p)_{nf} = (1-\varphi)(\rho C_p)_f + \varphi(\rho C_p)_s \quad (8)$$

And the thermal conductivity of the nanofluid k_{nf} for spherical nanoparticles can be written as

$$\frac{k_{nf}}{k_f} = \frac{(k_s + 2k_f) - 2\phi(k_f - k_s)}{(k_s + 2k_f) + \phi(k_f - k_s)} \quad (9)$$

The thermal expansion coefficient of nanofluid can determine by

$$(\rho\beta)_{nf} = (1-\varphi)(\rho\beta)_f + \varphi(\rho\beta)_s \quad (10)$$

Also the effective dynamic viscosity of the nanofluid given by

$$\mu_{nf} = \frac{\mu_f}{(1-\varphi)^{2.5}}, \quad (11)$$

Where the subscripts nf, f and s represent the thermo physical properties of the nanofluid, base fluid and the nanosolid particles respectively and ϕ is the solid volume fraction of the nanoparticles. The thermo physical properties of the nanofluid are given in Table 1.

Table – 1

Physical properties	Fluid phase	CuO (Copper)	Al_2O_3 (Alumina)	TiO_2 (Titanium dioxide)
C_p(j/kg K)	4179	385	765	686.2
ρ(kg m^3)	997.1	8933	3970	4250
k(W/m K)	0.613	400	40	8.9538
βx10^{-5} 1/k)	21	1.67	0.63	0.85

Since the flow is unidirectional, the continuity of equation (1) reduces to

$\frac{\partial u}{\partial x} = 0$ Where u is the axial velocity implies u = u(y)

The momentum, energy and diffusion equations in the scalar form reduces to

$$-\frac{\partial p}{\partial x} + \left(\frac{\mu_{nf}}{\delta}\right)\frac{\partial^2 u}{\partial y^2} - \frac{\rho_{nf}\delta F}{\sqrt{k}}u^2 - \rho_{nf}g - \left(\frac{\mu}{k}\right)u = 0 \quad (12)$$

$$(\rho_0 C_p)_{nf}\, u\frac{\partial T}{\partial x} = k_{nf}\frac{\partial^2 T}{\partial y^2} + Q(T_o - T) \quad (13)$$

$$u\frac{\partial C}{\partial x} = D_1\frac{\partial^2 C}{\partial y^2} - k_1 C + k_{11}\frac{\partial^2 T}{\partial y^2} \tag{14}$$

The relevant boundary conditions are

$$u = 0, \quad T=T_w, \quad C=C_w \text{ at } \quad y=\pm L \tag{15}$$

Following Tao [34] and Das et al [8] we assume that the temperature and concentration of the both walls is $T_w = T_0 + Ax$, $C_w = C_0 + Bx$ where A and B are the vertical temperature and concentration gradients which are positive for buoyancy –aided flow and negative for buoyancy –opposed flow, respectively, T_0 and C_0 are the upstream reference wall temperature and concentration respectively. For the fully developed laminar flow in the presences of radial magnetic field, the velocity depend only on the radial coordinate and all the other physical variables except temperature, concentration and pressure are functions of y and x, x being the vertical co-ordinate

The temperature and concentration inside the fluid can be written as

$$T = T^{\bullet}(y) + Ax \quad , \quad C = C^{\bullet}(y) + Bx$$

We define the following non-dimensional variables as

$$u' = \frac{u}{(\nu / L)},\ (x', y') = (x, y)/L\ ,\ \ p' = \frac{p\delta}{(\rho\nu^2 / L^2)},\ \ \theta(\mathrm{y}) = \frac{\mathrm{T^{\bullet}\text{-}T_0}}{\mathrm{ALP_1}},\ \ \mathrm{C} = \frac{\mathrm{C^{\bullet}\text{-}C_0}}{\mathrm{BLP_1}} \tag{16}$$

$$A_1 = \frac{1}{(1-\varphi)^{2.5}},\ \ A_2 = (1-\varphi) + \varphi(\frac{\rho_s}{\rho_f}),\ \ A_3 = 1-\varphi+\varphi\frac{(\rho C_p)_s}{(\rho C_p)_f},\ \ A_4 = 1-\varphi+\varphi(\frac{(\rho\beta)_s}{(\rho\beta)_f},\ \ A_5 = \frac{k_{nf}}{k_f}$$

Introducing these non-dimensional variables the governing equations in the dimensionless form reduce to (on dropping the dashes)

$$A_1\frac{d^2u}{dy^2} = 1 + \delta(A_1 D^{-1})u - \delta G A_4(\theta) - \delta^2 A_2 \Delta u^2 \tag{17}$$

$$A_5\frac{d^2\theta}{dy^2} - \alpha\theta = (A_2 A_3 P_r)u \tag{18}$$

$$\frac{d^2C}{dy^2} - (\gamma Sc)C = (Sc)u \tag{19}$$

Where

$$\Delta = FD^{-1/2}\left(\text{Inertia or Forchheimer parameter}\right) \qquad P_r = \frac{\mu_f C_{pf}}{k_f}\left(\text{Prandtl Number}\right)$$

$$G = \frac{\beta_f g A L^3}{\nu_f^2} \quad \text{(Grashof Number)} \qquad \gamma = \frac{k_1 L^2}{\nu_f} \quad \text{(Chemical reaction parameter)}$$

$$\alpha = \frac{QL^2}{k_f}\left(\text{Heat source parameter}\right) \quad Sc = \frac{\nu}{D_B} \quad \text{(Schmidt number)}$$

The corresponding boundary conditions are

$$u = 0 \ \ , \ \ \theta = 0 \ \ , \ \ C = 0 \quad on\ y = \pm 1 \tag{20}$$

3. FINITE ELEMENT ANALYSIS

To solve these differential equations with the corresponding boundary conditions, we assume if u^i, θ^i, c^i are the approximations of u, θ and C we define the errors (residual) E_u^i, E_θ^i, E_c^i as

$$E_u^i = \frac{d}{d\eta}\left(A_1 \frac{du^i}{d\eta}\right) - (A_1 D^{-1})u^i + \delta^2 A_2 (u^i)^2 - \delta A_4 G(\theta^i) \quad (21)$$

$$E_c^i = \frac{d}{dy}\left(\frac{dC^i}{dy}\right) - (\gamma Sc)C^i - Scu^i \quad (22)$$

$$E_\theta^i = \frac{d}{dy}\left(A_5 \frac{d\theta^i}{dy}\right) - A_2 A_3 P_r u^i) - \alpha\theta^i \quad (23)$$

Where

$$u^i = \sum_{k=1}^{3} u_k \psi_k, \quad C^i = \sum_{k=1}^{3} C_k \psi_k, \quad \theta^i = \sum_{k=1}^{3} \theta_k \psi_k \quad (24)$$

These errors are orthogonal to the weight function over the domain of e^i under Galerkin finite element technique we choose the approximation functions as the weight function. Multiply both sides of the equations (21-23) by the weight function i.e. each of the approximation function ψ_j^i and integrate over the typical three nodded linear element (η_e, η_{e+1}) we obtain

$$\int_{\eta_e}^{\eta_{e+1}} E_u^i \psi_j^i dy = 0 \qquad (i = 1,2,3,4,) \quad (25)$$

$$\int_{\eta_e}^{\eta_{e+1}} E_c^i \psi_j^i dy = 0 \qquad (i = 1,2,3,4,) \quad (26)$$

$$\int_{\eta_e}^{\eta_{e+1}} E_\theta^i \psi_j^i dy = 0 \qquad (i = 1,2,3,4,) \quad (27)$$

Where

$$\int_{\eta_e}^{\eta_{e+1}} \left(\frac{d}{d\eta}\left(A_1 \frac{du^i}{d\eta}\right) - (A_1 D^{-1})u^i + \delta^2 A_2 \mathrm{A}(u^i)^2 - \delta G A_4(\theta^i)\right) \psi_j^i dy = 0 \quad (28)$$

$$\int_{\eta_e}^{\eta_{e+1}} \left(\frac{d}{dy}\left(\frac{dC^i}{dy}\right) - (\gamma Sc) C^i - Scu^i\right)\psi_j^i dy = 0 \quad (29)$$

$$\int_{\eta_e}^{\eta_{e+1}} \left(\frac{d}{dy}\left(A_5 \frac{d\theta^i}{dy}\right) - A_2 A_3 P_r u^i - \alpha\theta^i\right)\psi_j^i dy = 0 \quad (30)$$

Following the Galerkin weighted residual method and integration by parts method to the equations (28) – (30) we obtain

$$\int_{\eta_e}^{\eta_{e+1}} A_1 \frac{d\Psi_j^i}{dy}\frac{d\psi^i}{dy} dy - \delta(A_1 D^{-1}) \int_{\eta_e}^{\eta_{e+1}} u^i \Psi_j^i dy + \delta^2 A_2 \int_{\eta_e}^{\eta_{e+1}} (u^i)^2 \Psi_j^i dy - \delta G A_4 \int_{\eta_e}^{\eta_{e+1}} (\theta^i)\Psi_j^i dy = Q_{1,j} + Q_{2,j} \quad (31)$$

Where – $Q_{1,j} = \Psi_j(\eta_e)\frac{du^i}{d\eta}(\eta_e)$ $\qquad$ $Q_{2,j} = \Psi_j(\eta_{e+1})\frac{du^i}{d\eta}(\eta_{e+1})$

IJETED

$$\int_{\eta_e}^{\eta_{e+1}} \frac{d\Psi_j^i}{dy}\left(\frac{dC^i}{dy}\right)dy-(\gamma Sc)\int_{\eta_e}^{\eta_{e+1}} C^i\psi_j^i dy+\frac{ScSo}{N}\int_{\eta_e}^{\eta_{e+1}} \frac{d\Psi_j^i}{dy}\left(\frac{d\theta^i}{dy}\right)\psi_j^i dy-Sc\int_{\eta_e}^{\eta_{e+1}} u^i\psi_j^i dy=R_{1,j}+R_{2,j} \quad (32)$$

Where – $R_{1,j}=\Psi_j(\eta_e)\frac{dC^i}{dy}(\eta_e) \qquad R_{2,j}=\Psi_j(\eta_{e+1})(\frac{dC^i}{dy}(\eta_{e+1})+(\eta_{e+1}))$

$$A_5\int_{\eta_e}^{\eta_{e+1}} \frac{d\Psi_j^i}{dy}\frac{d\theta^i}{dy}dy-A_2A_3P_r\int_{\eta_e}^{\eta_{e+1}} u^i\psi_j^i dy-\alpha\int_{\eta_e}^{\eta_{e+1}} \theta^i\psi_j^i dy=\mathrm{S}_{1,\mathrm{j}}+\mathrm{S}_{2,\mathrm{j}} \quad (33)$$

Where – $S_{1,j}=\Psi_j(\eta_e)\frac{d\theta^i}{dy}(\eta_e) \qquad S_{2,j}=\Psi_j(\eta_{e+1})\frac{d\theta^i}{dy}(\eta_{e+1})$

Making use of equations (24) we can write above equations as

$$A_1\sum_{k=1}^{3}u_k\int_{\eta_e}^{\eta_{e+1}}\frac{d\psi_j^i}{dy}\frac{d\psi_k}{dy}dy-\sum_{k=1}^{3}\delta(A_1D^{-1})u_k\int_{\eta_e}^{\eta_{e+1}}\psi_j^i\psi_k dy-\delta A_4G(\sum_{k=1}^{3}\theta_k\int_{\eta_e}^{\eta_{e+1}}\psi_j^i\psi_k dy\sum_{k=1}^{3}\psi_j^i\psi_k dy$$
$$+\delta^2\mathrm{A}_2\sum_{k=1}^{3}u_k^2\int_{\eta_e}^{\eta_{e+1}}\left(\frac{d\psi_k}{d\eta}\right)^2\psi_j^i dy=Q_{1,j}+Q_{2,j} \quad (34)$$

$$\sum_{k=1}^{3}C_k\int_{\eta_e}^{\eta_{e+1}}\frac{d\psi_j^i}{dy}\frac{d\psi_k}{dy}dy-(\gamma Sc)\sum_{k=1}^{3}C_k\int_{\eta_e}^{\eta_{e+1}}\psi_j^i\psi_k d\eta-Sc\sum_{k=1}^{3}C_k\int_{\eta_e}^{\eta_{e+1}}\psi_j^i\psi_k dy=R_{1,j}+R_{2.j} \quad (35)$$

$$A_5\sum_{k=1}^{3}\theta_k\int_{\eta_e}^{\eta_{e+1}}\frac{d\psi_j^i}{dy}\frac{d\psi_k}{dy}dy-A_2A_3P_r\sum_{k=1}^{3}u_k\int_{\eta_e}^{\eta_{e+1}}\psi_k\psi_j^i dy-\alpha\sum_{k=1}^{3}\theta_k\int_{\eta_e}^{\eta_{e+1}}\psi_k\psi_j^i dy=S_{1,j}+S_{2.j} \quad (36)$$

Choosing different Ψ_j^i's corresponding to each element η_e in the equation (34) yields a local stiffness matrix of order 3×3 in the form

$$A_1(f_{i,j}^k)(u_i^k)-\delta GA_4(g_{i.j}^k)(\theta_i^k)+\delta A_1D^{-1}(m_{i.j}^k)(u_i^k)+\delta^2A_2(n_{i.j}^k)(u_{i,j}^k)=(Q_{i,j}^k)+(Q_{2,j}^k) \quad (37)$$

Likewise the equation (35) & (36) gives rise to stiffness matrices

$$(e_{i,J}^k)(C_i^k)-Sc(m_{i.j}^k)(u_i^k)=R_{1J}^k+R_{2J}^k \quad (38)$$

$$A_5(l_{iJ}^k)(\theta_i^k)-(A_2A_3P_r)(t_{iJ}^k)(\theta_i^k)-\alpha(s_{iJ}^k)(\theta_i^k)=S_{1,J}^k+S_{2,J}^k \quad (39)$$

Where $\left(f_{i,J}^k\right)$, $\left(g_{i,J}^k\right)$, $\left(m_{i,J}^k\right)$, $\left(n_{i,J}^k\right)$, $\left(e_{i,J}^k\right)$, (s_{iJ}^k), $\left(t_{iJ}^k\right)$ are 3×3matrices and $\left(Q_{2,J}^k\right),\left(Q_{1,J}^k\right),\left(R_{2,J}^k\right),\left(R_{1J}^k\right),\left(S_{2J}^k\right)$ and $\left(S_{1J}^k\right)$ are 3×1 column matrices and such stiffness matrices (37) – (39) in terms of local nodes in each element are assembled using inter element continuity and equilibrium conditions to obtain the coupled global matrices in terms of the global nodal values of k, θ & C. In case we choose n-quadratic elements then the global matrices are of order 2n+1. The ultimate coupled global matrices are solved to determine the unknown global nodal values of the velocity, temperature and concentration in fluid region. In solving these global matrices an iteration procedure has been adopted to include the boundary and effects in the porous region.

The shape functions corresponding to

$$\Psi_1^1=\frac{(y-4)(y-8)}{32} \qquad \Psi_2^1=\frac{(y-12)(y-16)}{32} \qquad \Psi_3^1=\frac{(y-20)(y-24)}{32}$$

$$\Psi_1^2=\frac{(y-2)(y-4)}{8} \qquad \Psi_2^2=\frac{(y-6)(y-8)}{8} \qquad \Psi_2^3=\frac{(y-10)(y-12)}{8}$$

$$\Psi_1^3=\frac{(3y-4)(3y-8)}{32} \qquad \Psi_2^3=\frac{(3y-12)(3y-16)}{32} \qquad \Psi_3^3=\frac{(3y-20)(3y-24)}{32}$$

$$\Psi_1^4 = \frac{(y-1)(y-2)}{2} \qquad \Psi_2^4 = \frac{(y-3)(y-4)}{2} \qquad \Psi_3^4 = \frac{(y-5)(y-6)}{2}$$

$$\Psi_1^5 = \frac{(5y-4)(5y-8)}{32} \qquad \Psi_2^5 = \frac{(5y-12)(5y-16)}{32} \qquad \Psi_3^5 = \frac{(5y-20)(5y-24)}{32}$$

4. STIFFNESS MATRICES

The global matrix for θ, N and u are respectively

$$A_3 X_3 = B_3 \quad (40)$$
$$A_4 X_4 = B_4 \quad (41)$$
$$A_5 X_5 = B_5 \quad (42)$$

In fact, the non-linear term arises in the modified Brinkman linear momentum equation (28) of the porous medium. The iteration procedure of in taking the global matrices as follows, we split the square term into a product term and keeping one of them say u_i's under integration, the other is expanded in terms of local nodal values as in (24), resulting in the corresponding coefficient matrix $(n_i^k{}_j's)$ in (37), whose coefficients involve the unknown u_i's . To evaluated (38) to begin with choose the initial global nodal values of u_i's as zeros in the zeroth approximation. We evaluate u_i's , θ_i's and C_i's in the usual procedure mentioned earlier. Later choosing these values of u_i's as first order approximation calculate θ_i's, C_i's. In the second iteration, we substitute for u_i's the first order approximation of and u_i's and the first approximation of θ_i's and C_i's obtain second order approximation. This procedure is repeated till the consecutive values of u_i's , θ_i's and C_i's differ by a preassigned percentage. For computational purpose we choose five elements in flow region.

5. SHEAR STRESS, NUSSELT NUMBER AND SHERWOOD NUMBER

The shear stress, rate of heat transfer (Nusselt Number) and mass transfer (Sherwood Number) in non-dimensional form are

$$\tau_{y=\pm1} = \left(\frac{du}{dy}\right)_{y=\pm1}, \qquad Nu_{y=\pm i} = \left(\frac{d\theta}{dy}\right)_{y=\pm1} \qquad Sh_{y=\pm1} = \left(\frac{dC}{dy}\right)_{y=\pm1}$$

COMPARISON: In the absence of Heat Sources (α=0) the results are in good agreement with Madhusudhana Reddy et al [26].

Table - 2

Parameters		Reddy et al [26]			Present Results(α=0)		
		Cuo-Water			Cuo-Water		
ϕ	Δ	τ(-1)	Nu(-1)	Sh(-1)	τ(-1)	Nu(-1)	Sh(-1)
0.1	2	-0.0142988	-0.104039	0.9829	-0.014286	-0.103985	0.98289
0.3	2	-0.0272453	-0.199393	0.8672	-0.02718	-0.198895	0.86716
0.5	2	-0.0403833	-0.300521	0.7504	-0.04036	-0.30028	0.75038
0.1	4	-0.001412	-0.001028	---	-0.00139	-0.001025	---
0.1	6	-0.003381	-0.00558	---	-0.003372	-0.00589	---
0.1	10	-0.0075285	-0.02878	---	-0.007519	-0.02875	---

Table – 3

Parameters		Reddy et al [26]			Present Results(α=0)		
		Al_2O_3-Water			Al_2O_3-Water		
ϕ	Δ	τ(-1)	Nu(-1)	Sh(-1)	τ(-1)	Nu(-1)	Sh(-1)
0.1	2	-0.010483	-0.24113	0.9874	-0.010475	-0.24108	0.98738
0.3	2	-0.008218	-0.10006	1.0953	-0.008216	-0.10005	1.0952
0.5	2	-0.007971	-0.09043	1.1962	-0.007965	-0.09042	1.1961
0.1	4	-0.000574	-0.00078	---	-0.000573	-0.000775	---
0.1	6	-0.001306	-0.00458	---	-0.001384	-0.00456	---
0.1	10	-0.003038	-0.02223	---	-0.003035	-0.02221	---

6. DISCUSSION OF THE NUMERICAL RESULTS

A mathematical assessment for the numerical solution of this problem is performed, and the outcomes are illustrated graphically in Figures 2- 16. They explain the fascinating features of important parameters on the nanofluid velocity, temperature, concentration distributions, skin friction, Nusselt number and Sherwood number for two different types of water based nanofluids. As in [Oztop and Abu-Nada (2008)], we take the values of the nanofluid volume fraction ϕ in the range of $0 \le \phi \le 0.08$. We considered for the convective flow in a lid driven cavity, the value of the nanofluid volume fraction in the range $0 \le \phi \le 0.08$. If the concentration exceeds the maximum level of 0.08, sedimentation could take place. We have chosen here $\Pr = 6.2$ while G, D^{-1}, α, Δ, Sc, γ and ϕ are varied over a range, which are listed in the Figure legends.

Effects of parameters on velocity profiles:

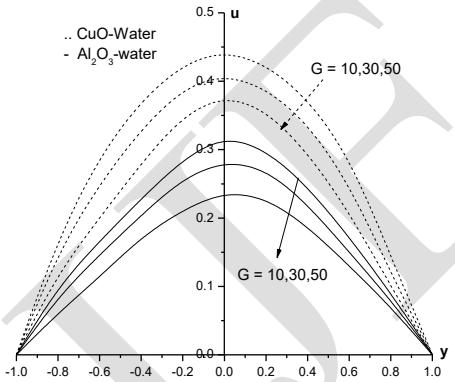

Fig: 2 Variation of u with G
D^{-1}=0.1, α=2, Δ=2, ϕ=0.1

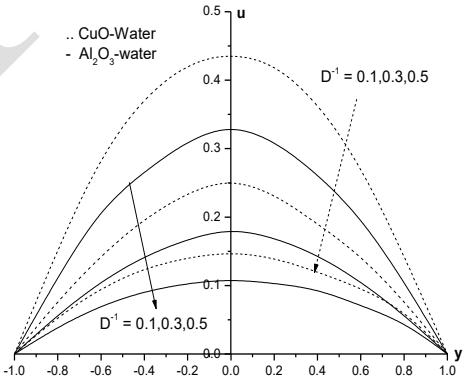

Fig.3 Variation of u with D^{-1}
G = 10, α=2, Δ=2, ϕ=0.1

Fig.2 represents the effect of Grashof number G on the nanofluid velocity profile. It is found that the nanofluid velocity field reduces with increase of Grashof number in both types of nanofluids. This is due to the fact that the thickness of the boundary layer reduces with increase in the thermal buoyancy parameter G. We also find that the nano fluid velocity in the case of CuO–water nanofluid is relatively greater than that of Al_2O_3-water. This phenomenon has good agreement with the physical realities. Fig.3 represents the effect of inverse Darcy parameter D^{-1} on the nanofluid velocity profile. It is observed from the figure that the velocity distribution decreases with increasing the inverse Darcy parameter D^{-1}. This is due to the fact that increase in the obstruction of the fluid motion with increase in the inverse Darcy parameter (since permeability of the porous medium appears in the denominator of the inverse Darcy parameter),thereby increase in inverse Darcy parameter indicates decrease in the permeability of the porous medium so the fluid velocity decrease. We also find that the

nanofluid velocity in the case of CuO – water nanofluid is relatively greater than that of Al_2O_3-water nanofluid. This phenomenon has good agreement with the physical realities.

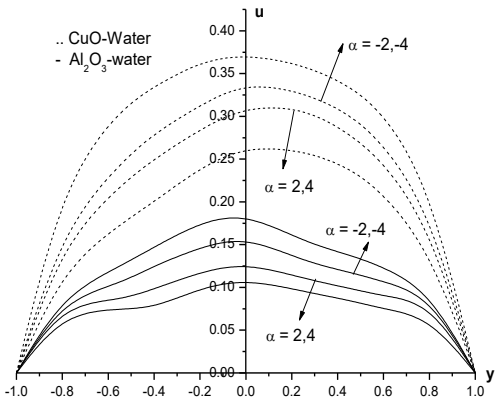

Fig.4 Variation of u with α
G = 10, D^{-1}=0.1, Δ=2, ϕ=0.1

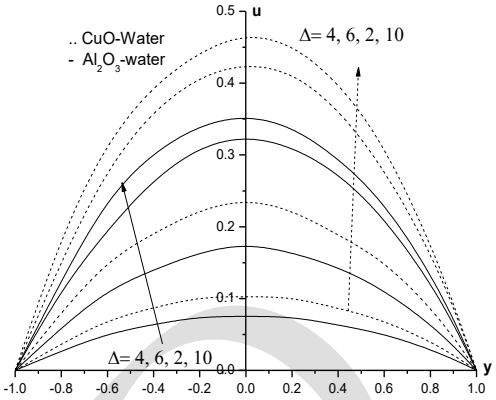

Fig.5 Variation of u with Δ
G = 10, D^{-1}=0.1, α=2, ϕ=0.1

Figs.4 depicts the behavior of the velocities with heat source parameter α. It is found that axial velocity exhibits a decreasing tendency with increase in the strength of the heat generating source. This is due to the fact that when heat is absorbed, the buoyancy forces decreases which reduces the flow rate and there by gives rise to a depreciation in the velocity profile .An increase in the heat absorbing heat source increases the axial velocity in the entire flow region in both types of nanofluids. We also find that the values velocity in CuO-water nanofluid is relatively higher than that of Al_2O_3-water nanofluid. The variation of velocity with Forchheimer number Δ is exhibited in Fig.5. It is found that velocity shows depreciation with increasing the values of Forchheimer number Δ≤4 and for further higher Δ ≥6, we notice an increase in the velocity in the flow region. This is due to the fact that the thickness of the boundary layer reduces with smaller values of Δ ≤4 and increases with higher values of Δ≥6 in both types of nanofluid. Fig.6 display the effect of nanoparticle volume fraction ϕ on the nanofluid velocity and. It is found that as the nanoparticle volume fraction increases the nanofluid velocity experiences an enhancement in the boundary layer. These Figures illustrate this agreement with the physical behavior. When the volume of the nanoparticle increases the thermal conductivity and the thermal boundary layer thickness increases. We also notice that the nanofluid velocity in the case of Al_2O_3–water nanofluid is relatively lesser than that of CuO-water nanofluid.

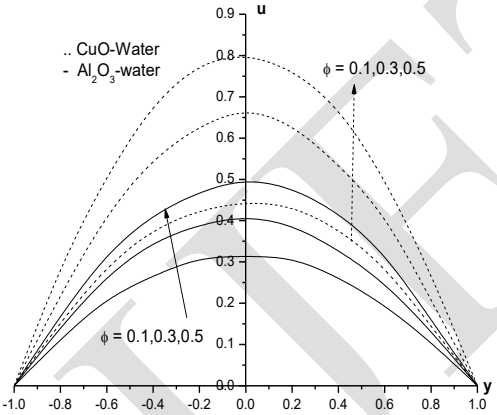

Fig.6 Variation of u with ϕ
G = 10, D^{-1}=0.1, α=2, Δ=2

Effects of parameters on Temperature profiles:

We follow the convention that the non-dimensional temperature is positive / negative according as the actual temperature greater/lesser than the equilibrium temperature.

Fig.7 represents the temperature with thermal buoyancy parameter G. It can be seen from the profiles that an increase in G enhances the actual temperature in the entire flow region. This is due to the fact that the thermal buoyancy enhances the thickness of the thermal boundary layer in both types of nanofluids. Also we find that the temperature in Al_2O_3-water is relatively lesser than that of CuO-water fluid. Fig.8 represents the effect of inverse Darcy parameter D^{-1} on the nanofluid temperature profile. It is observed from the figure that the actual temperature distribution increases with increasing values of D^{-1} as a result of increase in the thickness of the thermal boundary layer owing to the Darcy drag developed by the

porous medium. We also find that the nanofluid temperature in the case of CuO – water nanofluid is relatively greater than that of Al_2O_3-water nanofluid. This phenomenon has good agreement with the physical realities.

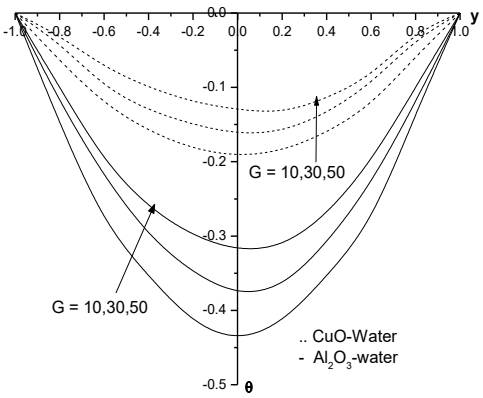

Fig.7 Variation of θ with G
D^{-1}=0.1, α=2, Δ=2, ϕ=0.1

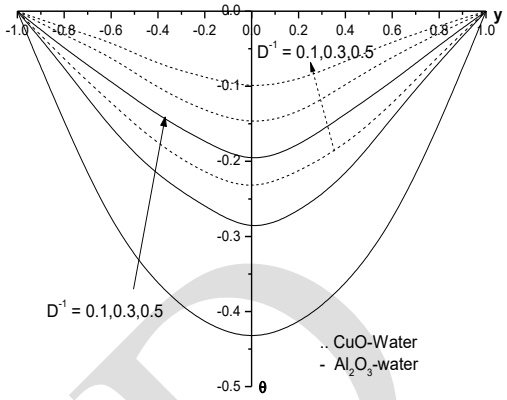

Fig.8 Variation of θ with D^{-1}
G = 10, α=2, Δ=2, ϕ=0.1

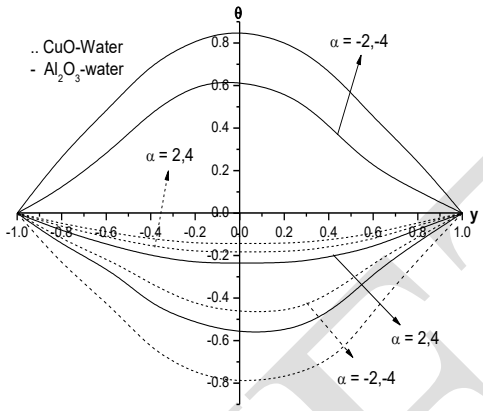

Fig.9 Variation of θ with α
G = 10, D^{-1}=0.1, Δ=2, ϕ=0.1

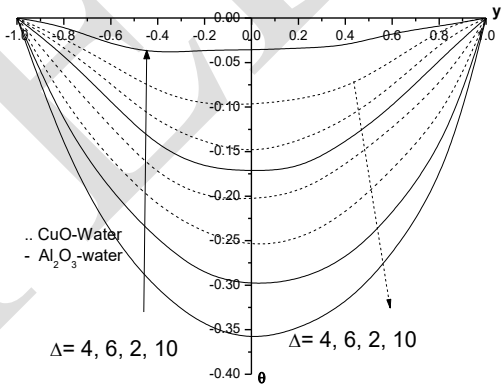

Fig.10 Variation of θ with Δ
G = 10, D^{-1}=0.1, α=2, ϕ=0.1

Fig.9 depicts the behavior of the temperature with heat source parameter α. It is found that actual temperature exhibits an increasing tendency with increase in the strength of the heat generating source. This is due to the fact that the presence of the heat source generates energy in the thermal boundary layer and as a consequence the temperature rises. In the case of heat absorption (α<0) the actual temperature falls with decreasing values of α<0 owing absorption of energy in the thermal boundary layer in both types of nanofluid. We also find that the values actual temperature in CuO-water nanofluid is relatively higher than that of Al_2O_3-water nanofluid. Fig.10 shows the variation of temperature with Δ. It is found that an increase in Δ≤4 enhances the actual temperature in the thermal boundary layer and for higher values of Δ≥6 we notice a reduction in the actual temperature. Thus, the inclusion of inertia and boundary effects enhances the temperature in the flow region. We also note that the temperature in Al_2O_3-water nanofluid is relatively smaller than that of CuO-water nanofluid.

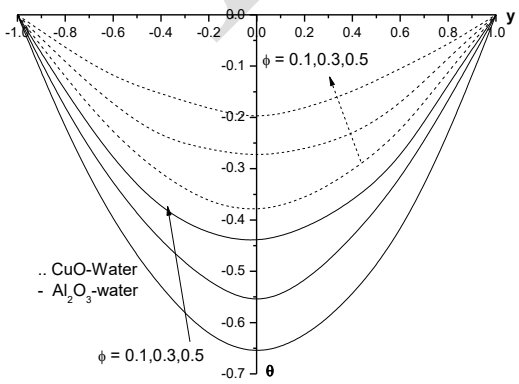

Fig.11 Variation of θ with ϕ
G = 10, D^{-1}=0.1, α=2, Δ=2

Fig.11 shows that the variation of temperature with ϕ. It can be seen from the profiles that an

increase in the nanoparticle volume fraction reduces the actual temperature in the boundary layer. This is due to the fact that the thickness of the thermal boundary layer decreases with increase in ϕ. Also we find that the actual temperature in Al_20_3-water is relatively lesser than that of CuO-water fluid.

Effects of parameters on Concentration profiles:

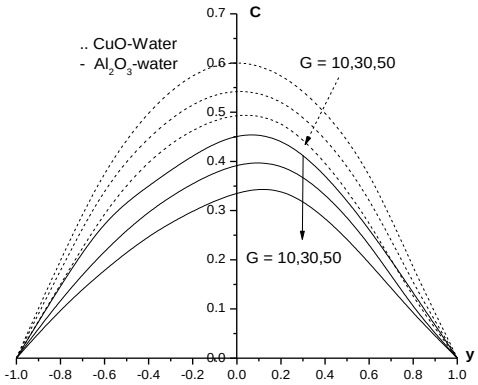

Fig.12 Variation of C with G
D^{-1}=0.1, Sc=1.3, γ_0=0.5, ϕ=0.1

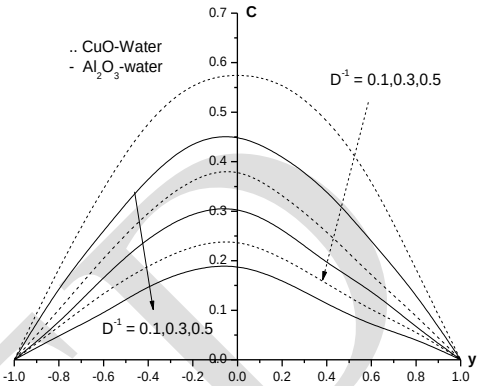

Fig.13 Variation of C with D^{-1}
G = 10, Sc=1.3, γ_0=0.5, ϕ=0.1

Fig.12 represents the concentration(C) with Grashof number G. It can be seen from that the effect of increasing thermal buoyancy parameter is to diminish the concentration throughout the solutal boundary layer. This is attributed to the fact that an enhancement in the thermal buoyancy parameter results in the reduction of the thickness of the solutal boundary layer. We find that values of concentration in Al2o3-water nanofluid are relatively smaller than those in CuO-water nanofluid. Fig.13 represents the effect of inverse Darcy parameter D^{-1} on the nanofluid concentration profile. It is observed from the figure that the concentration distribution decreases with increasing values of D^{-1} as a result of decreasing the thickness of the solutal boundary layer owing to the Darcy drag developed by the porous medium. We also find that the nano-fluid concentration in the case of CuO-water nanofluid is relatively greater than that of Al_2O_3-water nanofluid. This phenomenon has good agreement with the physical realities.

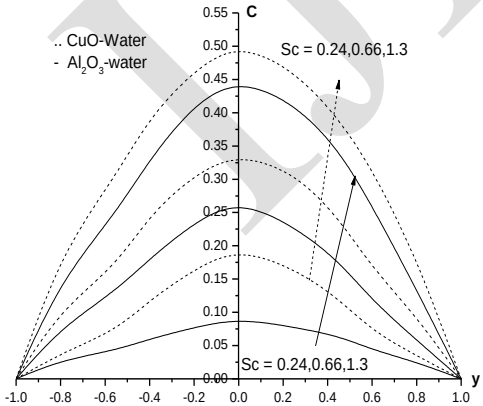

Fig.14 Variation of c with Sc
G = 10, D^{-1}=0.1, γ_0=0.5, ϕ=0.1

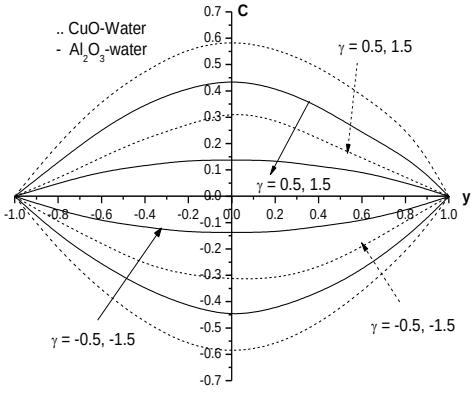

Fig.15 Variation of C with γ_0
G = 10, D^{-1}=0.1, Sc=1.3, ϕ=0.1

The variation of concentration with Schmidt number Sc shows that lesser the molecular diffusivity larger the concentration in the flow region in both types of nanofluid. Also the concentration in CuO-water nanofluid is relatively higher than those in Al_2O_3-water nanofluid (fig.14).The effect of chemical reaction (γ_0) on C is shown in fig.15. It can be observed from the profiles that the concentration reduces in the degeneration chemical

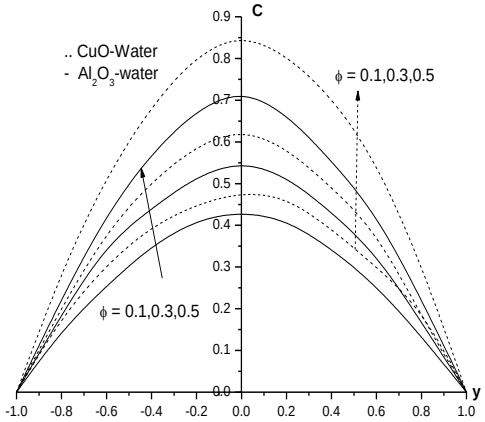

Fig.16 Variation of C with ϕ
G = 10, D^{-1}=0.1, Sc=1.3, γ_s0.5

reaction case and increases in the generating chemical reaction case. Also we find that the nanofluid concentration in the case of CuO-water nanofluid is relatively greater than that of Al_2O_3-water nanofluid.

Fig.16 shows the variation of concentration with nanoparticle volume fraction ϕ. We notice a reduction in the concentration with increase in ϕ. This may be attributed to the fact that an enhancement in ϕ results in increasing the thickness of the solutal boundary layer. The concentration in CuO-water nanofluid is higher than those values of C in Al_2O_3-water nanofluid

Effects of parameters on Skin friction:

Table – 4

Parameters		Cuo-Water		Al_2O_3-Water	
		$(\tau)_{y=+1}$	$(\tau)_{y=-1}$	$(\tau)_{y=+1}$	$(\tau)_{y=-1}$
G	10	0.0162093	-0.0142988	0.0119033	-0.0104835
	30	0.0159967	-0.0139305	0.0119079	-0.0105424
	50	0.0158544	-0.0128999	0.0120979	-0.0106278
D^{-1}	0.1	0.0162093	-0.0142988	0.0119033	-0.0104835
	0.3	0.0083689	-0.0083686	0.0060974	-0.0060895
	0.5	0.0060588	-0.0079470	0.0044021	-0.0057657
α	2	0.0162093	-0.0142988	0.0119033	-0.0104835
	4	0.0161894	-0.0142754	0.0043933	-0.0057585
	-2	0.0163186	-0.0143795	0.0043431	-0.0057174
	-4	0.0165188	-0.0145443	0.0043661	-0.0057361
ϕ	0.1	0.0162093	-0.0142988	0.0119033	-0.0104835
	0.3	0.0310306	-0.0272453	0.0074749	-0.0082180
	0.5	0.0466166	-0.0403833	0.0064953	-0.0079705
Δ	2	0.0162093	-0.0142988	0.0119033	-0.0104835
	4	0.0171074	-0.0162075	0.0150951	-0.0125026
	6	0.0391748	-0.0344822	0.0251264	-0.0210956
	10	0.0854013	-0.0753128	0.0550952	-0.0452329

The table 4 displays the behavior of local skin friction (τ) at the walls y=±1. It is found that an increase in thermal buoyancy parameter G reduces skin friction at both the walls in CuO-water nanofluid while Al_2O_3-water nanofluid the skin friction enhances with increase in G. An increase in inverse Darcy parameter D^{-1} reduces skin friction at the walls in both types of nanofluid. The variation of τ with heat source parameter (α) shows that the skin friction decreases at both the walls with increase in the strength of heat generating source (α>0) while an increase in the heat absorption heat source (α<0) we notice an enhancement in τ at y=±1. An increase in the nano particle volume fraction ϕ enhances τ at the walls in CuO-water nanofluid and reduces it in Al_2O_3-water nanofluid. With respect to Forchheimer number Δ we find an enhancement in the magnitude of the skin friction τ at the walls in both types of

nanofluid. Thus, the inclusion of inertia and boundary effects increases the skin friction at the wall. From the tabular values of the skin friction w.r.to different parametric variations we find that the magnitude of skin friction in CuO-water nanofluid is relatively greater than those values in Al_2O_3-water nanofluid.

Effects of parameters on Nusselt Number:

Table – 5

Parameters		Cuo-Water		Al_2O_3-Water	
		$(Nu)_{y=+1}$	$(Nu)_{y=-1}$	$(Nu)_{y=+1}$	$(Nu)_{y=-1}$
G	10	-0.067302	-0.104039	-0.015596	-0.241131
	30	-0.066844	-0.103948	-0.015103	-0.241265
	50	-0.065817	-0.101764	-0.014842	-0.241606
D^{-1}	0.1	-0.067302	-0.104039	-0.015596	-0.241131
	0.3	-0.033751	-0.052182	-0.007761	-0.119966
	0.5	-0.022528	-0.034821	-0.005170	-0.079847
α	2	-0.067302	-0.104039	-0.015596	-0.241131
	4	-0.054143	-0.083731	-0.002934	-0.150264
	-2	-0.013131	-0.203034	0.009803	0.151697
	-4	-0.025191	-0.389534	0.013993	0.161859
ϕ	0.1	-0.067302	-0.104039	-0.015596	-0.241131
	0.3	-0.072895	-0.199393	-0.006479	-0.100062
	0.5	-0.087433	-0.300521	-0.005799	-0.090438
Δ	2	-0.067302	-0.104039	-0.015596	-0.241131
	4	-0.068168	-0.110345	-0.016751	-0.256795
	6	-0.068894	-0.126113	-0.017503	-0.264691
	10	-0.070874	-0.168983	-0.019441	-0.302593

The local Nusselt number (Nu) at the walls $y=\pm1$ is shown in table 5 for a different parametric variations. It is found that an increase in G reduces the Nusselt number at $y=\pm1$ in CuO-water nanofluid. In Al_2O_3-water nanofluid the Nusselt number at $y=+1$ reduces with G and enhances at $y=-1$. An increase in D^{-1} reduces the rate of heat transfer at both the walls in both types of nanofluid. The variation of Nu with heat source parameter α shows that the rate of heat transfer at $y=\pm1$ reduces with increase in the strength of heat generating source while in the case of heat absorption source, we notice an enhancement in Nu at both the walls in both types of nanofluid. An increase in the Nano particle volume fraction ϕ increase Nu at $y=\pm1$ in CuO-water nanofluid and reduces it Al_2O_3-water nanofluid. The variation of Nu with Forchheimer number Δ shows that the magnitude of Nu increases with increase in Δ at $y=\pm1$ in both types of nanofluids. From the tabular values of Nusselt number w.r.to G, D^{-1}, ϕ and Δ we find that the values of CuO-water nanofluid are higher than those values in Al_2O_3-water nanofluid at y= +1, while at y= -1 the values of CuO-water nanofluid are relatively lesser than those values of Al_2O_3-water nanofluid. Also we find that the values of Nu at $y=+1$ in CuO-water nanofluid are relatively greater than those values in Al_2O_3-water nanofluid for both heat generating/absorbing source. The values of Nu at $y=-1$ in CuO-water nanofluid are relatively lesser than those values in Al_2O_3-water nanofluid for $\alpha>0$, While a reversed effect is noticed in the behavior of Nu for $\alpha<0$.

Effects of parameters on Sherwood Number:

The table 6 represents the variation of mass transfer Sh at y=±1 with different values of G, D^{-1}, Sc, γ and ϕ.

Table – 6

Parameters		Cuo-Water		Al_2O_3-Water	
		$(Sh)_{y=+1}$	$(Sh)_{y=-1}$	$(Sh)_{y=+1}$	$(Sh)_{y=-1}$
G	10	0.0211231	0.9884	0.0155152	0.9894
	30	0.0208243	1.0832	0.0155109	1.0874
	50	0.0206537	1.1833	0.0154836	1.1888
D^{-1}	0.1	0.0211231	0.9884	0.0155152	0.9894
	0.3	0.0105459	1.0916	0.0076862	1.0931
	0.5	0.0069493	1.1949	0.0050521	1.1983
Sc	0.24	0.0039722	1.1968	0.0009368	1.1993
	0.6	0.0108819	1.0912	0.0025819	1.0981
	1.3	0.0211231	0.9884	0.0155152	0.9894
γ	0.5	0.0211231	0.9884	0.0155152	0.9894
	1.5	0.0070077	1.0945	0.0015655	1.0993
	-0.5	-0.021328	1.0176	-0.0050786	1.0045
	-1.5	-0.007111	1.0059	-0.0017449	1.0017
ϕ	0.1	0.0211231	0.9884	0.0155152	0.9894
	0.3	0.0404749	0.8672	0.0083389	1.0953
	0.5	0.0610183	0.7504	0.0076500	1.1962

It is found that an increase in G reduces |Sh| at y=+1 and enhances at y= −1 in both types of nanofluid. |Sh| at y=+1 in CuO-water nanofluid is relatively greater than that of Al_2O_3-water nanofluid. |Sh| at y=−1 in CuO-water nanofluid are relatively lesser than those values in Al_2O_3-water nanofluid. An increase D^{-1} reduces |Sh| at y=+1 and |Sh| enhances at y=−1 in both types of nanofluid. Also we find that |Sh| at y= +1 in CuO-water nanofluid is relatively higher than those values in Al_2O_3-water nanofluid. At y=−1 we noticed reverse effect in the behavior of |Sh|. With respect to Schmidt number Sc we find that an increase in Sc enhances |Sh| at y=+1 and reduces at y=−1 in both types of nanofluid. |Sh| at y=+1 in CuO-water nanofluid are relatively greater than those of Al_2O_3-water nanofluid. At y=−1 we noticed reverse effect in the behavior of |Sh|. The rate of mass transfer with Chemical reaction parameter γ at y=+1 reduces in magnitude in both degenerating and generating chemical reaction cases. While at y= -1, Sh enhances in the degenerating chemical reaction case and reduces in the generating chemical reaction case in both types of fluid. We find that the values of |Sh| at y=+1 in CuO-water nanofluid are relatively greater than those values in Al_2O_3-water nanofluid. The values of Sh at y=−1 in CuO-water nanofluid are relatively lesser than those values in Al_2O_3-water nanofluid for γ>0, While a reversed effect is noticed in the behavior of |Sh| for γ<0. The variation of Sh with Nano particle volume fraction ϕ shows that the rate of mass transfer enhances at y=+1 and recues at y=−1 with increase in ϕ in CuO-water nanofluid. In Al_2O_3-water nanofluid |Sh| reduces at y=+1 and enhances at y=−1. Also we notice that the values of |Sh| at y=+1 in CuO-water nanofluid are relatively greater than those of Al_2O_3-water nanofluid. While at y=−1 |Sh| in CuO-water nanofluid are relatively lesser than those of Al_2O_3-water nanofluid.

7. CONCLUSIONS:

The coupled equations governing the flow, heat and mass transfer have been solved by using Galerkin finite method with quadratic approximation functions. The velocity, temperature and concentration have been analyzed for different parametric variations. The important conclusions of the analysis are

- An increase in Grashof number G reduces the velocity, concentration and enhances actual temperature in the flow region. The skin friction reduces at both the walls in CuO-water nanofluid and enhances in Al_2O_3-water nanofluid. The rate of heat transfer (Nu) reduces at both the walls in CuO-water nanofluid and Nu reduces at y=+1 in Al_2O_3-water nanofluid and a reverse effect is noticed at y=−1. The Sherwood number reduces at y=+1 and enhances at y= −1 in both types of fluid.
- Lesser the permeability of porous medium smaller the velocity, Concentration and larger the temperature. The skin friction and rate of heat transfer reduces at both walls in both types of nanofluid. The rate of mass transfer reduces at y=+1 and enhances at y= −1 in both types of fluid.
- An increase in $\alpha>0$ reduces the velocity and enhances the actual temperature, while a reversed effect is observed in the case of $\alpha<0$. The skin friction and Nusselt number reduces for $\alpha>0$ and enhances for $\alpha<0$ at y= ±1.
- An increase in nanoparticle volume fraction ϕ enhances the velocity, actual temperature and concentration. The skin friction and rate of heat transfer enhances in CuO-water nanofluid and reduces in Al_2O_3-water nanofluid at both walls. The rate of mass transfer enhances at y= +1 and reduces at y= -1 in CuO-water nanofluid. The Sherwood number reduces at y= +1 and enhances at y= -1 in Al_2O_3-water nanofluid.
- An increase in Forchheimer number (Δ) leads to depreciation in velocity and actual temperature with increase in $\Delta\leq4$ and for further higher $\Delta\geq6$; we notice an enhancement in velocity and actual temperature. The skin friction and rate of heat transfer enhances at both the walls in both types of fluid.
- Lesser the molecular diffusivity larger the concentration. The rate mass transfer (Sh) enhances at y= +1 and reduces at y= -1 in both type of fluids.
- The concentration reduces in the degeneration chemical reaction case ($\gamma>0$) and enhances in the generating chemical reaction case ($\gamma<0$) in both types of fluids. The rate of mass transfer (Sh) at y=+1 reduces in magnitude in both degenerating and generating chemical reaction cases, while at y= -1, Sh enhances in the degenerating chemical reaction case and reduces in the generating chemical reaction case in both types of fluid.

8. REFERENCES

[1] Basant K.Jha, Muhammad L.Kaurangini: Approximate analytical solutions for the nonlinear Brinkman-Forchheimer-extended Darcy flow model. Applied Mathematics, 2 pp. 1432-1436 (2011).
[2] Beckermann, C. Visakanta, R and. Ramadhyani, S: A numerical study of non-Darcian natural convection in a vertical enclosure filled with a porous medium, Numerical Heat transfer 10, pp.557-570, (1986).
[3] Buongiorno, J: Convective transport in nanofluids, ASME J. Heat Transfer 128 pp.240-250(2006).
[4] Cheng: Heat transfer in geothermal systems. Adv.Heat transfer 14, pp. 1-105(1978).

[5] Choi, S.U.S., ASME FED 231/MD, Enhancing Thermal Conductivity of Fluids with Nanoparticles, Developments and applications of Non-Newtonian Flow, Vol.66,, pp:99-105(1995).
[6] Choi, S.U.S., Zhang, Z.G., Yu, W., Lockwood, F.E., and Grulke, E.A: Anomalously thermal conductivity enhancement in nanotube suspensions, Appl. Phys. Lett. 79 (2001) 2252-2254.
[7] Das, S.K., Choi, S.U.S., Yu, W., Pradeep, T: Nanofluids: Science and Technology, Wiley, New Jersey, 2007.
[8] Das, S., Jana, R.N. and Makinde, O.D: Mixed convective magnetohydrodynamic flow in a vertical channel filled with Nanofluid., Eng. Sci. and Technology-an International journal;,V,18,pp.244-255(2015).
[9] Daungthongsuk, W., Wongwises, S: A critical review of convective heat transfer nanofluids, Renew. Sustain. Energy Rev. 11, pp. 797-817 (2007).
[10] Dulal Pal, Hiranmoy Mondal: Hydromagnetic non-Darcy flow and heat transfer over a stretching sheet in the presence of thermal radiation and Ohmic dissipation. Communications in Nonlinear Science and Numerical Simulations, 15, pp. 1197-1209 (2010).
[11] Fakour, M., Vahabzadeh, A., Ganji, D. D: Scrutiny of mixed convection flow of a nanofluid in a vertical channel, Case Stud. Therm. Eng. 4 pp.15-23 (2014).
[12] Grosan, T., Pop, I: Fully developed mixed convection in a vertical channel filled by a nanofluid, J. Heat Transfer 134 (8) 082501(2012).
[13] Jang, S.P., Choi, S.U.S: Effects of various parameters on nanofluid thermal conductivity, ASME J. Heat Transfer, 129, pp. 617-623(2007).
[14] Kalidas, N and Prasad, V: Benard convection in porous media Effects of Darcy and Prandtl Numbers, Int. Syms. Convection in porous media, non-Darcy effects, proc.25th Nat. Heat Transfer Conf. V.1, pp.593-604 (1988).
[15] Kang Ki, J.Y.T., Choi, C.K.: Analysis of convective instability and heat transfer characteristics of nanofluids, Phys. Fluids, 16 pp.2395-2401(2004).
[16] Kiblinski, P., Phillpot, S.R., Choi, S.U.S., Eastman, J.A: Mechanism of heat flow is suspensions of nano-sized particles (nanofluids), Int. J. Heat Mass Transfer, 42, pp. 855-863(2002).
[17] Laurait, G and Prasad, V. : Natural convection in a vertical porous cavity a numerical study of Brinkman extended Darcy formulation., J. Heat Transfer, pp.295-320(1987).
[18] Madhusudhana Reddy, Y., Rama Krishna, G.N., Prasada Rao, D.R.V: Finite element analysis of mixed convective heat and mass transfer flow of nanofluid in vertical channel, International Journal of Advanced Scientific and Technical Research, vol. 1, Issue 7, January –February (2017).
[19] Maghrebi, M.J., Nazari, M., Armaghansi, T: Forced convection heat transfer of nanofluids in a porous channel, Transp. Porous Media 93 pp.401-413(2012).
[20] Maïga, S.E.B., Nguyen, C.T., Galanis, N., Roy, G: Heat transfer behaviors of nanofluids in a uniformly heated tube, Superlatt. Microstruct. 35, pp.543-557(2004).
[21] Maïga, S.E.B., Palm, S.J., Nguyen, C.T., Roy, G., Galanis, N: Heat transfer enhancement by using nanofluids in forced convection flows, Int. J. Heat and Fluid Flow, 26, pp. 530-546(2005).
[22] Nakayamma, A and Shenoy, A.V: A unified similarity transformation for Darcy and non-Darcy forced-free and mixed convection heat transfer in non-Newtonian inelastic fluid saturated porous media, The Chemical Engineering Journal, 50, pp. 33-45(1992).

[23] Nield, D.A., Kuznetsov, A.V: Forced convection in a parallel -plate channel occupied by a nanofluid or a porous medium saturated by a nanofluid, Int. J. Heat Mass Transfer, 70, pp.430-433(2014).
[24] Polidori, G., Fohanno, S., Nguyen, C.T: A note on heat transfer modeling of Newtonian nanofluids in laminar free convection, Int. J. Therm. Sci., 46, pp.739-744(2007).
[25] Poulikakos D., and Bejan, A.: The Departure from Darcy flow in Nat. Convection in a vertical porous layer, physics fluids V.28, pp. 3477-3484 (1985).
[26] Prasad, V and Tuntomo, A: Inertia Effects on Natural Convection in a vertical porous cavity, numerical Heat Transfer, V.11, pp. 295-320 (1987).
[27] Rossi di Schio, E., Celli, M., Barletta, A: Effect of Brownian diffusion and thermophoresis on the laminar forced convection of a nanofluid in a channel, ASME J. Heat Transfer, 136, 022401(2013).
[28] Sacheti, N.C., Chandran, P., Singh, A.K., Bhadauria, B.S: Transient free convective flow of a nanofluid in a vertical channel, Int. J. Energy Technol, 4, pp.1-7(2012).
[29] Seyyedi, S.M., Bararnia, H., Ganji, D.D., Gorji-Bandpy, M., Soleimani, S : Numerical investigation of the effect of a splitter plate on forced convection in a two dimensional channel with an inclined square cylinder, Int. J. Therm. Sci. 61 (0), pp.1-14(2012).
[30] Sheikholeslami, M., Gorji-Bandpy, M., Ganji, D.D., Soleimani, S., Seyyedi, S.M: Natural convection of nanofluids in an enclosure between a circular and a sinusoidal cylinder in the presence of magnetic field, Int. Commun. Heat Mass Transfer, 39 (9), pp.1435-1443(2012).
[31] Sheikholeslami, M., Hatami, M., Ganji, D.D: Analytical investigation of MHD nanofluid flow in a semi-porous channel, Powder Technol. 246 (0), pp.327-336(2013).
[32] Sheikholeslami, M., Ganji, D.D: Magnetohydrodynamic flow in a permeable channel filled with nanofluid, Sci. Iran. B 21 (1) pp.203-212(2014).
[33] Soleimani, S., Sheikholeslami, M., Ganji, D.D., Gorji- Bandpay, M: Natural convection heat transfer in a nanofluid filled semi-annulus enclosure, Int. Commun. Heat Mass Transfer 39 (4) (2012) 565-574.
[34] Tao, L.N: On combined and forced convection in channels, ASME J. Heat Transfer, V.82, pp.233-238(1960).
[35] Tien, D., and Hong, J.T: Natural convection in porous media under non-Darcian and non-uniform permeability conditions, hemisphere, Washington. C. (1985).
[36] Tong, T.L and Subramanian, E.: A boundary layer analysis for natural correction in porous enclosures: use of the Brinkman-extended Darcy model, Int. J. Heat Mass Transfer.28,pp.563-571 (1985).
[37] Trisaksri, V., Wongwises, S: Critical review of heat transfer characteristics of nanofluids, Renew. Sustain. Energy Rev. 11, pp. 512-523(2007).
[38] Vafai, K., Tien, C.L: Boundary and Inertia effects on flow and Heat Transfer in Porous Media, Int. J. Heat Mass Transfer, V.24, pp.195-203 (1981).
[39] Vafai, K., Thyagaraju, R.: Analysis of flow and heat Transfer at the interface region of a porous medium, Int. J. Heat Mass Trans., V.30, pp.1391-1405 (1987).
[40] Wang, X., Xu, X., Choi, S.U.S: Thermal conductivity of nanoparticle fluid mixture, J. Thermophys. Heat Transfer 13, pp.474-480(1999).
[41] Xu Hang, Pop, I: Fully developed mixed convection flow in a vertical channel filled with nanofluids, Int. Commun. Heat Mass Transfer, 39, 1086-1092(2012).

[42] Xu, H., Fan, T., Pop, I: Analysis of mixed convection flow of a nanofluid in a vertical channel with the Buongiorno mathematical model, Int. Commun. Heat Mass Transfer 44 (2013) 15-22.
[43] Zhengwen Zeng and Reid Grigg.: A criterion for Non-Darcy flow in porous media, Transport in Porous Media. 63, pp. 57-69(2006).

IJETED